Journal of Materials Chemistry C

Accepted Manuscript

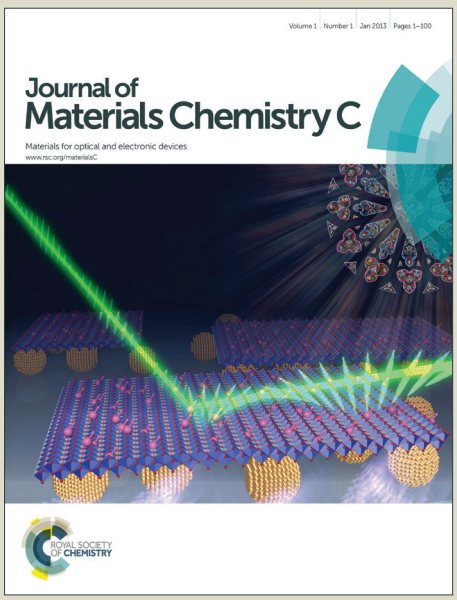

ROYAL SOCIETY OF CHEMISTRY

www.rsc.org/materialsC

Journal Name

RSCPublishing

COMMUNICATION

Plasmonics-enhanced metal-organic framework nanoporous films for highly sensitive near-infrared absorption†

Cite this: DOI: 10.1039/x0xx00000x

Received 00th January 2012,
Accepted 00th January 2012

DOI: 10.1039/x0xx00000x

www.rsc.org/

Ki-Joong Kim,‡[a] Xinyuan Chong,‡[b] Peter B. Kreider,[a] Guoheng Ma,[a] Paul R. Ohodnicki,[c] John P. Baltrus,[c] Alan X. Wang*[b] and Chih-Hung Chang*[a]

Combined plasmonic nanocrystals and metal-organic framework thin-films are fabricated for sensing gases in the near-infrared range. This nanocomposite thin-film shows a highly sensitive response in near-infrared absorption, which is attrributed to preconcentration of gas molecules in metal-organic framework pores causing close proximity to the electromagnetic fields at the plasmonic nanocrystals surface.

Substantial recent research has been focused on the synthesis and characterization of nanoporous metal-organic framework (MOF) materials with high internal surface areas.[1] MOFs, which are hybrid materials composed from organic linkers and metal ions, have demonstrated excellent properties for gas purification, separation, and storage.[2] In addition, nanoporous MOF thin films are particularly useful in chemical sensing due to their tunability and structural diversity.[3] MOF thin films can be used to rapidly adsorb guest gases within material pores and can be recycled simply by subjecting them to dynamic vacuum or flowing inert gases for a short time because most guest gases are physisorbed to MOF pores. Various approaches including solvachromism/vaporchromism,[4] luminescence,[5] interferometry,[6] reflectance,[7] localized surface plasmon resonance spectroscopy,[8] impedance,[9] piezoresistive microcantilever[10] and quartz crystal microbalance[11] have been reported for the use of MOFs for sensing. Despite the high potential of the aforementioned sensors using MOFs, the lack of a highly sensitive and specific signal transduction method has limited their implementation.

Infrared absorption sensors play pivotal roles in analytical chemistry, allowing the quantitative detection of small amounts of molecules and the identification of molecular structures and conformational states. In recent years, chip-scale near-infrared (NIR) absorption sensors have been developed for low-concentration gas detection due to the wide availability and low cost of optoelectronic devices for telecommunication applications.[12] The biggest challenge in the field is that most gases do not have fundamental vibration bands in the NIR wavelength range, and hence these devices have relatively low detection sensitivity. As a result, the ability to increase signal strength in the NIR range from selected gases through the use of new functional materials and innovative optical engineering will significantly improve the sensitivity of these sensors.

Plasmonics is a flourishing field of science and technology that exploits the unique optical properties of metallic nanostructures to route and manipulate light in nanometer length scales.[13] In recent years, plasmonic materials have been exploited for optical gas sensing by monitoring modifications to the plasmonic behavior in real time.[13b-13e] Plasmonic nanocrystals (NCs) have also demonstrated orders of magnitude improvement in sensitivity for surface-enhanced Raman scattering (SERS)[14] and surface-enhanced infrared absorption (SEIRA)[15]. Until now, most SEIRA studies have critically evaluated the noble metals such as gold nanoantennas,[15b-15e] as these have been shown to enhance IR vibrational signals with monolayer sensitivity. It is worth noting that the use of doped metal oxides also have potential as SEIRA materials. Transparent conducting oxides such as Indium-tin oxide (ITO) nanocrystals (NCs) have unique surface plasmon resonance (SPR) properties in the NIR region where the peak wavelength can be easily tuned by controlling the amount of tin doping, for example.[16a-16c] If the SPR peak could be fine-tuned to match the overtune of the vibration bands of gas molecules at NIR wavelengths, sensitive NIR absorption gas sensors could be explored based upon the SEIRA concept with enhanced selectivity as compared to optical sensors based upon monitoring real-time changes of absorption in plasmonic materials due to free carrier density changes.[16d,16e] To further increase low detection sensitivity, we report here for the first time, a metal oxide-based plasmonics-enhanced MOF film with high NIR absorption for CO_2, which is crucial for biological, energy and environmental systems.

With these motivations, we have fabricated plasmonics-enhanced nanoporous films consisting of ITO NCs and MOF. A Cu-BTC (BTC = benzene-1,3,5-tricarboxylic acid) MOF was chosen as a model compound because it is the most widely studied MOF material in thin-film form[6a] and has good adsorption capacity for CO_2.[1f,3c] Plasmonic ITO NCs were first synthesized using a hot-injection method and deposited on substrates *via* spin-coating, followed by growth of the Cu-BTC MOF using the room temperature layer-by-layer (LBL) approach (more details in experimental section, ESI†). Fig. 1 shows the absorption spectra of the ITO NCs dispersed in tetrachloroethylene (TCE) with varying Sn percentages. No surface plasmon resonance (SPR) was observed in the un-doped sample (In_2O_3 NCs), while an absorption peak did appear with the ITO NCs. This is due to the SPR absorption and this property provides strong evidence that the Sn occupies substitutional sites creating free-electrons in the In_2O_3 structure. The SPR peak is gradually blue-shifted from 2400 to 1610 nm when the Sn precursor increased from 0.8% to 10%. A gradual red shift of the SPR peak from 1810 to 2550 nm was observed as the %Sn increased from 15 to 20% (insert of Fig. 1). This is due to the high concentration of tin dopants, which cause significant lattice distortion, and/or decreases the electron density resulting in a lower SPR frequency.[16b,-16d] These results indicate that 10% Sn-doped ITO NCs have the strongest plasmon absorption due to the corresponding highest free-electron density and therefore they were used for this study. Transmission electron microscopy (TEM) imaging (Fig. 2B) shows that ITO NCs were highly mono-dispersed and high-resolution TEM (HRTEM, insert of Fig. 2B) reveals single crystals with a lattice fringe distance of 0.292 nm, illustrative of the crystal lattice spacing of the (222) planes of ITO.

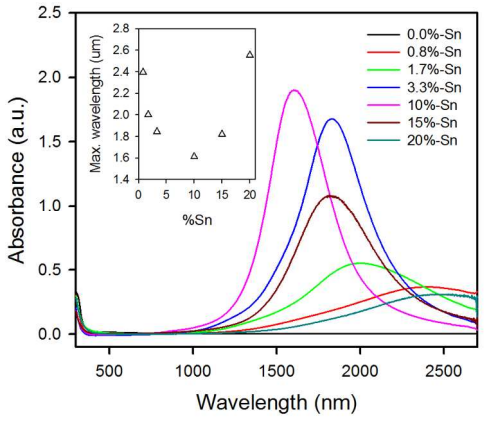

Fig. 1 (A) Absorption spectra of as-synthesized ITO NCs dispersed in TCE (inset shows a dependence of the SPR peaks of ITO NCs on the doped %Sn).

Freshly prepared 10% Sn-doped ITO NCs were deposited onto a sapphire substrate by spin coating from a hexane solution, followed by O_2 plasma treatment and then Cu-BTC MOF film growth using the LBL method (Fig. 2A). Sapphire was chosen as a substrate because it is highly transparent to wavelengths of light from UV to mid IR ranges. The SEM image in Fig. 2C shows that the individual ITO NCs were uniformly deposited onto the sapphire substrate by the spin-coating method with the thickness of ~130 nm measured by cross-sectional SEM imaging (Fig. 2G). The residual organic compounds left on the surface of the ITO NCs should be removed prior to MOF film growth because the presence of organic compounds can have a negative effect not only on uniform MOF growth but also on the optical properties of the fabricated sensors. In this study, we used O_2 plasma techniques to remove any residual organic compounds (Fig. 2D) and to produce hydroxylated (-OH) surfaces, which could replace the self-assembled monolayer (SAM) commonly used in MOF thin-film growth[17] *via* the stepwise, LBL method. After 10 cycles of Cu-BTC MOF LBL growth on ITO film (MOF10//ITO) surfaces, crystals with sizes ranging from 150 nm to 300 nm were distributed on the surface of the ITO film (Fig. 2E and Fig. S1, ESI†). The single crystals had a clear triangular shape (insert of Fig. 2E). This suggests that the Cu-BTC particles grow with a specific orientation on the ITO film. Increasing to 30 cycles of Cu-BTC MOF LBL growth (MOF30//ITO) increases surface coverage into the continuous film region, shown in Fig. 2F. This suggests that the Cu-BTC MOF film grows directly on the ITO film after O_2 plasma treatment. The thickness of the Cu-BTC film was about 300 nm after 30 cycles of LBL growth (cross-sectional SEM image in Fig. 2G). Uniform thin films with complete surface coverage can be achieved by increasing the number of LBL growth cycles.

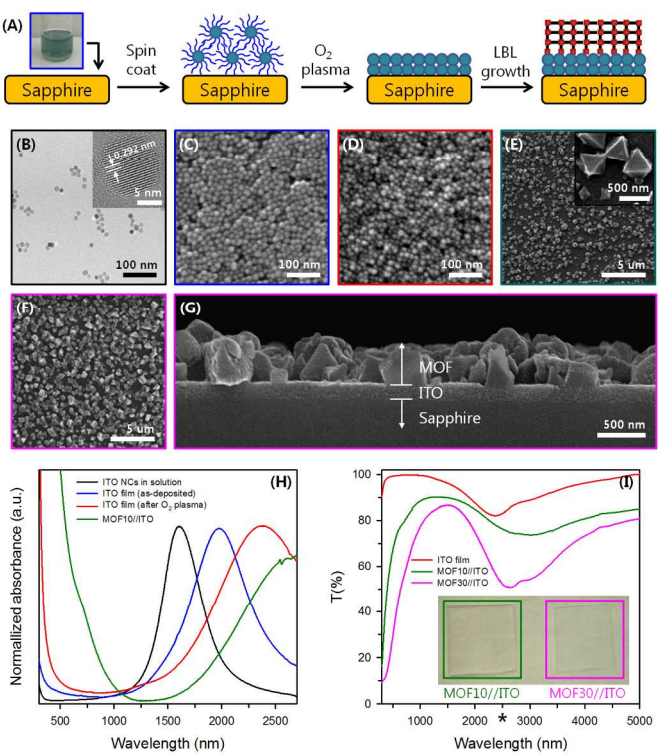

Fig. 2 (A) Schematic diagram for the preparation of MOF//ITO/Sapphire. (B) TEM image of the 10% Sn-doped ITO NCs in hexane (insert of HRTEM image). SEM images of the (C) as-deposited ITO film onto sapphire substrate by spin-coating, (D) ITO film on sapphire after O_2 plasma treatment, (E) 10 cycles (inset shows an individual Cu-BTC microcrystal with the size of ~300 nm), (F) 30 cycles Cu-BTC MOF grown onto ITO film using the LBL method. (G) Cross-sectional view SEM image of 30 cycles Cu-BTC MOF. (H) UV-Vis-NIR spectra of the 10% Sn-doped ITO NCs dispersed in TCE (black line), as-deposited ITO film on sapphire substrate by spin-coating (blue line), ITO film on sapphire after O_2 plasma treatment (red line),

and 10 cycles MOF grow on ITO film using the LBL method (green line). (I) Transmittance of the 10-cycles and 30-cycles LBL grown/ITO films (Inset shows the photo-images of MOF10//ITO and MOF30//ITO, respectively). This wide range spectrum was obtained by combining a spectrum recorded by a visible/NIR spectrophotometer (400 - 2700 nm) and FT-IR (2500 - 10000 nm). The symbol (*) on x-axis indicates the junction point between the two spectra (Vis-NIR and IR).

The UV-Vis-NIR absorption spectra of the samples obtained at each stage of film deposition and processing are shown in Fig. 2H. The absorption peak of the as-deposited 10% Sn-doped ITO film shifted to longer wavelength due to an increasing ITO volume fraction between particles from extremely low in the solvent dispersion to the as-deposited film,[16a] which is also observed in other samples with different %Sn (Fig. S2, ESI†). Additionally, a shift of the absorption peak after O_2 plasma treatment is observed. X-ray photoelectron spectroscopy (XPS) was employed to study the change of chemical states of the ITO film due to O_2 plasma treatment (Fig. S3, ESI†). It can be seen that the O 1s spectrum appears primarily as a single peak with a slight increase in peak broadening towards the higher binding energy side after O_2 plasma treatment (Fig. S3C, ESI†). Peak broadenings were also observed for the In 3d and Sn 3d spectra, although it is more obvious for the In 3d spectra. The increase in relative O 1s peak height of the ITO films after O_2 plasma-treatment suggests a higher concentration of oxygen (O/In = 1.31 *vs* 1.13 for the as-deposited ITO film) which is expected to impact the free carrier density. It is therefore concluded that the shift in absorption peak after O_2 plasma treatment is attributed to a decrease in free carrier concentration.

The MOF10//ITO shows a shoulder absorption band located at around 700 nm (Fig. 2H), which is attributed to the *d-d* band typical of copper carboxylate complexes,[18] indicating that the Cu-BTC MOF can be produced on the ITO film. The surface plasmon absorption peaks for an ITO NC film appears at 2400 nm and both were broadened and shifted towards a max value of ~2700 nm after Cu-BTC MOF growth on the ITO film (Fig. 2I). These results indicate that the surface plasmon frequencies are sensitive to their surrounding environment. It is worth noting that one of the overtone vibration frequencies for CO_2 molecules appears at 2700 nm and the spectrum of prepared nanoporous MOF//ITO thin-film in this study has significant overlap with this characteristic band of CO_2. Therefore, we expect this material to be very useful for the detection of CO_2 molecules in the NIR range.

The crystal structures of the samples were identified by XRD and the results are shown in Fig. 3. Both the as-deposited and O_2 plasma-treated ITO film show diffraction peaks at 2θ = 30.5° and 35.3° for (222) and (400) planes, respectively, corresponding to the cubic bixbyite structure of In_2O_3 (JCPDS file 06-0416).[19] At 10 cycles LBL growth of Cu-BTC MOF on the ITO film, a new diffraction peak at 2θ = 11.6° appears, corresponding to (222) plane of Cu-BTC. With a further increase of LBL growth cycles (MOF30//ITO), the diffraction peaks clearly reveal the presence of a polycrystalline material with preferred orientation along the (111) direction. Although the exact mechanism for the growth of Cu-BTC MOF on the surface of metal oxides is not completely understood, it has often been suggested that O_2 plasma treatment forms -OH groups on metal oxide surfaces.[17] The presence of -OH functional groups on the ITO film surface may induce MOF growth in a specific crystallographic direction, leading to preferentially oriented films. This result is in very good agreement with oriented growth using a thiol-based -OH terminated SAM.[20] Meanwhile, the decreasing intensity of ITO diffraction peaks indicates increased MOF layer thickness. This result further enforces the success of our strategy and this is the first demonstration of successful growth of MOF on an ITO surface *via* a stepwise LBL method, to our knowledge.

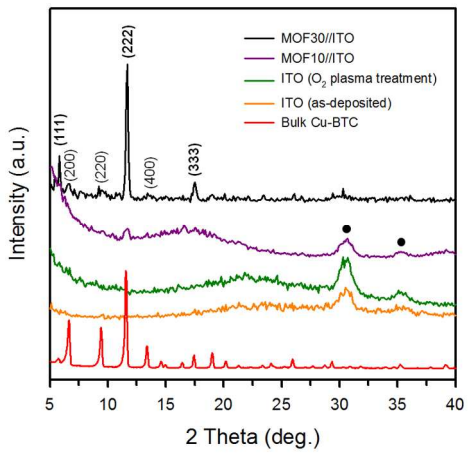

Fig 3 XRD patterns of the as-deposited (orange), O_2 plasma-treated (green) ITO film, 10 cycles (purple), and 30 cycles (balck) LBL Cu-BTC MOF growth onto ITO film. Bulk Cu-BTC MOF prepared by typical solvothermal reaction is shown for reference (red). Circle dots represent a cubic bixbyite structure of In_2O_3.

To examine the capability of the fabricated NIR absorption sensor, we designed a gas-flow cell that consisted of bare sapphire, ITO/sapphire or MOF//ITO/sapphire as shown in Fig. S4, ESI†. Before measuring the transmittance (%T), the designed flow-cell was inserted into the FT-IR chamber filled with pure N_2 gas in order to prevent the absorption of atmospheric CO_2. At the same time, the gas-cell was purged with ultra-high purity Ar gas for 24 hrs at room temperature in order to acquire a baseline spectrum. A high- (100%) or low-concentration (0.1%) of CO_2 gas was then passed through the flow-cell at atmospheric pressure. Typical FT-IR absorption spectra of CO_2 gases measured at the high and low concentrations of CO_2 using the flow cell without the MOF and ITO films are shown in Fig. S5, ESI†. We first investigated the sensor performance at a high-concentration of flowing CO_2 by measuring the difference in %T, which is calculated by (%T of Sapphire) - (%T of ITO/Sapphire or MOF//ITO/Sapphire). As can be seen in Fig. 4A (bottom), the difference in %T observed for an ITO film was about 0.8% compared to bare sapphire. In considering the possible simple increase in %T to be a result of the porous structure of the ITO NCs film, we first verified this using pure In_2O_3 NCs deposited onto sapphire a substrate with the same thickness as the ITO films. No difference in %T was observed, even with a porous structure. Next, we employed the HITRAN database and calculated the maximum absorption coefficient of 100% CO_2 to be around 2.7 μm, which is about 6 cm^{-1}. Then according to the

Beer-Lambert Law ($I = I_o\ exp(-\alpha\ell)$), the absorption due to a 130 nm pathlength is only 0.0078%, which is two orders of magnitude lower than the measured value of 0.8%. Therefore we concluded that the 0.8% difference in %T is the result of plasmonic effect of ITO NCs, which can enhance the sensitivity of CO_2 sensing.

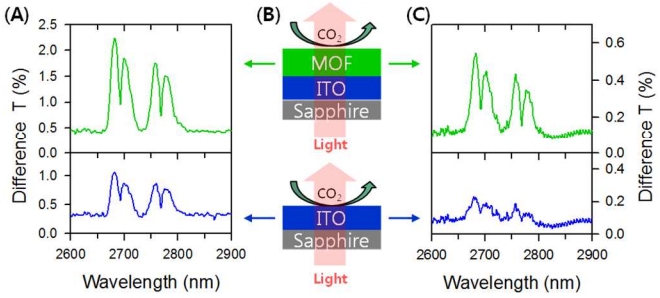

Fig. 4 Difference in %T at (A) high (100%) and (C) low (0.1%) concentration of CO_2 flowing on ITO/Sapphire and MOF//ITO/Sapphire samples. (B) Schematic diagram of CO_2 flowing on the (bottom) ITO/Sapphire and (top) MOF//ITO/Sapphire samples (See more detailed set-up in Fig. S4 in ESI).

Using a 3D finite element method simulation with periodic boundary condition, the electromagnetic field distribution of the ITO NCs thin film covered by a 90 nm MOF layer was quantitatively estimated by the RF module of COMSOL 4.4 (Fig. 5). Strong field enhancement mainly occurs in the gaps between ITO NCs, which form the hotspots. The maximum enhancement factor is about 755 and 762 for horizontal and vertical cross-sections, respectively. Since each gap has a hotspot, there will be intense hotspots across the whole array, which will contribute to the enhancement of NIR absorption. To compare the average enhancement, the optical field intensity was integrated over the 90 nm thick MOF layer. The results showed that with the presence of ITO NCs, the average enhancement factor will be about 50. Moreover, if a multilayer configuration is considered, the number of hotspots and average enhancment will further increase.

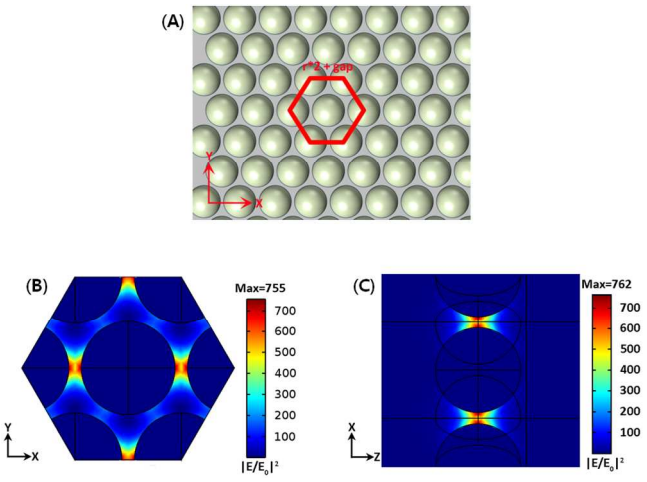

Fig. 5 3D FEM simulation of ITO NCs array. (A) Schematic of simulation model and electric field intensity distribution on (B) XY and (C) XZ plane at λ = 2700 nm. Model in the simulation was constructed according to the SEM image shown in Fig. 2C. For the sake of simplicity, we assumed that the ITO NCs formed a highly packed monolayer on top of the sapphire substrate (n_{sub} = 1.726), which is a hexagonal array as shown in Fig. 5A. The field was calculated at the incident light wavelength of 2700 nm. Fig. 5B and Fig. 5C present the map of simulated electric field intensity on horizontal (XY plane) and vertical (XZ plane) cross-sections. *E* is the local electric field and E_0 is the incident electric field. The incident light, excited from the substrate side, is polarized in the x-direction and propagates in the z-direction. The diameter of ITO NC was set at 15 nm with a 2 nm gap between each NC, which matches the average value of real synthesized NCs. A 90nm MOF layer was placed on top of ITO NPs with refractive index n_{MOF} = 1.3, which was obtained from ellipsometry. The dielectric constant of ITO is obtained from the Drude model.

The MOF30//ITO shows a 1.05% difference in %T (Fig. 4A (top)) compared to ITO, which is due to CO_2 readily adsorbing into MOF pores. Moreover, the difference in %T of sapphire and MOF30//ITO samples is about 1.85%. This value is in very good agreement with the sum of differences in %T of the two samples. Subsequently, the capability of the NIR absorption sensor at low concentration of flowing CO_2 was investigated and the results are shown in Fig. 4C. The difference in %T for the absorption band of CO_2 was also confirmed when the ITO NCs are coated onto the sapphire substrate (Fig. 4C (bottom)), confirming a plasmon enhancement effect, and implying that plasmonic ITO thin-films can detect low-concentrations of CO_2 well below 1000 ppm in the NIR range. Moreover, the difference in %T result of the MOF30//ITO film with low concentration of flowing CO_2 shows it can much more effectively detect CO_2 due to substantially increased sensitivity compared to the ITO film (Fig. 4C (top)). It should be noted that in order to further avoid the possible influence of residual CO_2 in MOF pores, all the samples were purged with Ar gas for 72 hrs at room temperature and tests were performed using a freshly corrected base-line before measuring %T. For reference, the flow cell designed in this study can be recovered within 60 min under the given conditions (Fig. S6, ESI†). The fabricated MOF//ITO sensor shows potential for applications in NIR gas sensing. Notably, this is the first example of a MOF thin film-based NIR absorption spectrum obtained for CO_2 gas at a wavelength of 2700 nm.

In summary, we demonstrated the fabrication of a plasmonics-enhanced MOF nanoporous film and its potential for sensing CO_2 in the NIR range. This nanocomposite thin film was highly sensitive for NIR absorption by effectively pre-concentrating CO_2 molecules in MOF pores resulting in the gas's close proximity to the strongly localized optical fields at the plasmonic NCs surface. We believe the combination of MOF and plasmonic NCs could overcome the grand challenges of low sensitivity at NIR wavelengths and enhance the selectivity that plagues other gas sensor materials.

This technical effort was performed in support of the National Energy Technology Laboratory's ongoing research under the RES contract DE-FE0004000. The authors would like to thank Zhen Fang for O_2 plasma treatment. Neither the United States Government nor any agency thereof, nor any of their employees, makes any warranty, express or implied, or assumes any legal liability or responsibility for the accuracy, completeness, or usefulness of any information, apparatus, product, or process disclosed, or represents that its use would not infringe privately owned rights. Reference herein to any specific commercial

Notes and references

[a] School of Chemical, Biological Environmental Engineering, Oregon State University, Corvallis, OR 97331, United States. E-mail: chih-hung.chang@oregonstate.edu
[b] School of Electrical Engineering and Computer Science, Oregon State University, Corvallis, OR 97331, United States. E-mail: wang@eecs.oregonstate.edu
[c] National Energy Technology Lab, United States Department of Energy, Pittsburgh, PA 15236, United States.

† Electronic Supplementary Information (ESI) available: Experimental details on plasmonics-enhanced MOF nanoporous films fabrication and characterization, further SEM, UV-Vis-NIR, XPS results, schematic of designed flow cell set-up, general CO_2 absorption spectra, and recovery test of the flow cell. See DOI: 10.1039/c000000x/

‡ These authors contributed equally to this work.

1 (a) P. Nugent, Y. Belmabkhout, S. D. Burd, A. J. Cairns, R. Luebke, K. Forrest, T. Pham, S. Ma, B. Space, L. Wojtas, M. Eddaoudi, M. J. Zaworotko, *Nature,* 2013, **495**, 80; (b) J. A. Bohrman, M. A. Carreon, *Chem. Commun*., 2012, **48**, 5130; (c) O. Shekhah, J. Liu, R. A. Fischer, C. Woll, *Chem. Soc. Rev*., 2011, **40**, 1081; (d) H. Furukawa, N. Ko, Y. B. Go, N. Aratani, S. B. Choi, E. Choi, A.O. Yazaydin, R. Q. Snurr, M. O'Keeffe, J. Kim, O. M. Yaghi, *Science,* 2010, **329**, 424; (e) J. R. Li, R. J. Kuppler, H. C. Zhou, *Chem. Soc. Rev*., 2009, **38**, 1477; (f) S. J. Dalgarno, P. K. Thallapally, L. J. Barbour, J. L. Atwood, *Chem. Soc. Rev*., 2007, **36**, 236.

2 (a) S.-L. Li, Q. Xu, *Energy Environ. Sci*., 2013, **6**, 1656; (b) J.R. Li, R. J. Kuppler, H.-C. Zhou, *Chem. Soc. Rev*., 2009, **38**, 1477; (c) G. Ferey, *Chem. Soc. Rev*., 2008, **37**, 191.

3 (a) E. Kreno, K. Leong, O. K. Farha, M. Allendorf, R. P. Van Duyne, J. T. Hupp, *Chem. Rev*., 2012, **112**, 1105; (b) B. Liu, *J. Mater. Chem*., 2012, **22**, 10094; (c) A. Betard, R. A. Fischer, *Chem. Rev*., 2012, **112**, 1055.

4 (a) Zhen-Zhong Lu, Rui Zhang, Yi-Zhi Li, Zi-Jian Guo, He-Gen Zheng, *J. Am. Chem. Soc*., 2011, **133**, 4172; (b) H. Lee, S. H. Jung, W. S. Han, J. H. Moon, S. Kang, J. Y. Lee, J. H. Jung, S. Shinkai, *Chem. Eur. J*., 2011, **17**, 2823; (c) P. D. Southon, L. Liu, E. A. Fellows, D. J. Price, G. J. Halder, K. W. Chapman, B. Moubaraki, K. S. Murray, J.-F. Letard, C. J. Kepert, *J. Am. Chem. Soc*., 2009, **131**, 10998.

5 (a) Y. Cui, Y. Yue, G. Qian, B. Chen, *Chem. Rev*., 2012, **112**, 1126; (b) M. D. Allendorf, C. A. Bauer, R. K. Bhaktaa, R. J. T. Houk, *Chem. Soc. Rev*., 2009, **38**, 1330.

6 (a) G. Lu, O. K. Farha, L. E. Kreno, P. M. Schoenecker, K. S. Walton, R. P. Van Duyne, J. T. Hupp, *Adv. Mater.,* 2011, **23**, 4449; (b) G. Lu, J. T. Hupp, *J. Am. Chem. Soc*., 2010, **132**, 7832.

7 (a) A. Demessence, C. Boissiere, D. Grosso, P. Horcajada, C. Serre, G. Ferey, G. J. A. A. Soler-Illia, C. Sanchez, *J. Mater. Chem*., 2010, **20**, 7676; (b) C. Boissiere, D. Grosso, S. Lepoutre, L. Nicole, A. B. Bruneau, C. Sanchez, *Langmuir,* 2005, **21**, 12362.

8 L. E. Kreno, J. T. Hupp, R. P. Van Duyne, *Anal. Chem.,* 2010, **82**, 8042.

9 S. Achmann, G. Hagen, J. Kita, I. M. Malkowsky, C. Kiener, R. Moos, *Sensors,* 2009, **9**, 1574.

10 M. D. Allendorf, R. J. T. Houk, L. Andruszkiewicz, A. A. Talin, J. Pikarsky, A. Choudhury, K. A. Gall, P. J. Hesketh, *J. Am. Chem. Soc*., 2008, **130**, 14404.

11 E. Biemmi, A. Darga, N. Stock, T. Bein, *Microporous Mesoporous Mater*., 2008, **114**, 380.

12 (a) W.-C. Lai, S. Chakravarty, A. X. Wang, C-Y Lin, R. T. Chen, *Opt. Lett*., 2011, **36**, 984; (b) J. T. Robinson, L. Chen, M. Lipson, *Opt. Express,* 2008, **16**, 4296.

13 (a) A. Comin, L. Manna, *Chem. Soc. Rev.,* 2014, **43**, 3957; (b) P. R. Ohodnicki, M. P. Buric, T. D. Brown, C. Matranga, C. Wang, J. Baltrus, M. Andio, *Nanoscale*, 2013, **5**, 9030; (c) P. R. Ohodnicki, C. Wang, S. Natesakhawat, J. P. Baltrus, T. D. Brown, *J. Appl. Phys*., 2012, **111**, 064320; (d) N. Karker, G. Dharmalingam, M. A. Carpenter, *ACS Nano*, 2014, **8**, 10953; (e) D. Buso, M. Post, C. Cantalini, P. Mulvaney, A. Martucci, *Adv. Funct. Mater*., 2008, **18**, 3843.

14 (a) Y. Hu, J. Liao, D. Wang, G. Li, *Anal. Chem*., 2014, **86**, 3955; (b) K. Sugikawa, S. Nagata, Y. Furukawa, K. Kokado, K.Sada, *Chem. Mater*., 2013, **25**, 2565; (c) K. Sugikawa, Y. Furukawa, K. Sada, *Chem. Mater*., 2011, **23**, 3132; (d) J. F. Li, Y. F. Huang, Y. Ding, Z. L. Yang, S. B. Li, X. S. Zhou, F. R. Fan, W. Zhang, Z. Y. Zhou, D. Y. Wu, B. Ren, Z. L. Wang, Z. Q. Tian, *Nature,* 2010, **464**, 392; (e) K. Kneipp, Y. Wang, H. Kneipp, L. T. Perelman, I. Itzkan, R. R. Dasari, M. S. Feld, *Phys. Rev. Lett*., 1997, **78**, 1667.

15 (a) M. Abb, Y. Wang, N. Papasimakis, C. H. de Groot, O. L. Muskens, *Nano Lett*., 2014, **14**, 346; (b) R. Adato, H. Altug, *Nat. Commun*., 2013, **4**, 2154; (c) D. Dregely, F. Neubrech, H. Duan, R. Vogelgesang, H. Giessen, *Nat. Commun*., 2013, **4**, 2237; (d) L. V. Brown, K. Zhao, N. King, H. Sobhani, P. Nordlander, N. J. Halas, J. Am. Chem. Soc., 2013, 135, 3688; (e) C. D'Andrea, J. Bochterle, A. Toma, C. Huck, F. Neubrech, E. Messina, B. Fazio, O. M. Marago, E. D. Fabrizio, M. L. de la Chapelle, P. G. Gucciardi, A. Pucci, *ACS Nano*, 2013, **7**, 3522.

16 (a) G. Garcia, R. Buonsanti, E.L. Runnerstrom, R. J. Mendelsberg, A. Llordes, A. Anders, T. J. Richardson, D. J. Milliron, *Nano Lett*., 2011, **11**, 4415; (b) M. Kanehara, H. Koike, T. Yoshinaga, T. Teranishi, *J. Am. Chem. Soc*., 2009, **131**, 17736; (c) Y. Jin, Q. Yi, Y. Ren, X.Wang, Z. Ye, *Nanoscale Res. Lett*., 2013, **8**, 153. (d) P. R. Ohodnicki, Jr., C. Wang, M. Andio, *Thin Solid Films*, 2013, **539**, 327; (e) P. R. Ohodnicki, Jr., C. Wang, M. Andio, *J. Appl. Phys*., 2014, **116**, 024309.

17 V. Stavila, J. Volponi, A. M. Katzenmeyer, M. C. Dixon, M. D. Allendorf, *Chem. Sci.,* 2012, **3**, 1531.

18 J. Nan, X. Dong, W. Wang, W. Jin, N. Xu, *Langmuir*, 2011, **27**, 4309.

19 R. A. Gilstrap Jr., C. J. Capozzi, C. G. Carson, R. A. Gerhardt, C. J. Summers, *Adv. Mater*., 2008, **20**, 4163.

20 (a) B. Liu, M. Tu, R. A. Fischer, *Angew. Chem. Int. Ed.,* 2013, **52**, 3402; (b) H. K. Arslan, O. Shekhah, J. Wohlgemuth, M. Franzreb, R. A. Fischer, C. Woll, *Adv. Funct. Mater.,* 2011, **21**, 4228; (c) A. Schodel, C. Scherb, T. Bein, *Angew. Chem. Int. Ed.,* 2010, **49**, 7225.

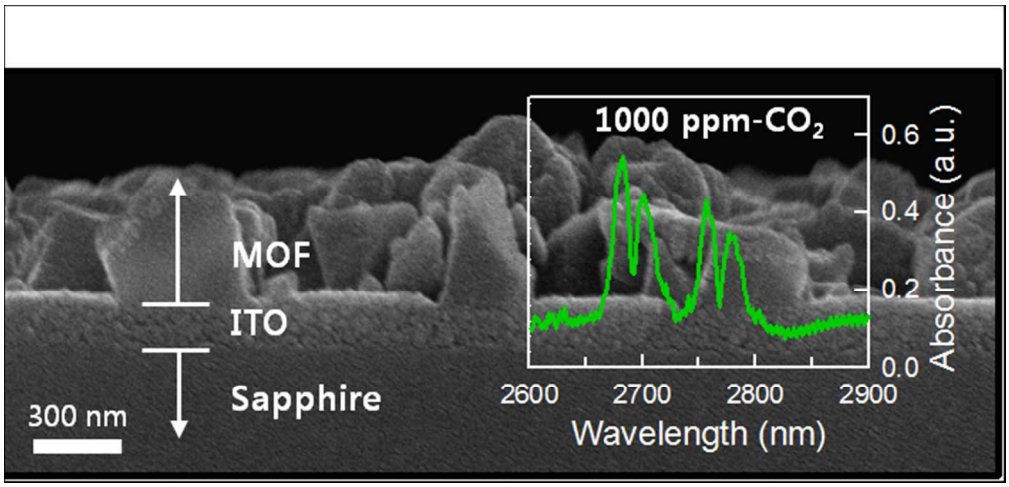

119x56mm (150 x 150 DPI)